

Article

A P-I Diagram Approach for Predicting Dynamic Response and Damage Assessment of Reactive Power Concrete Columns Subjected to Blast Loading

Qin Rong¹, Zhonghui Zhao^{1,*}, Xiaomeng Hou^{2,*}  and Zhizhong Jiang¹

¹ School of Architecture and Civil Engineering, Harbin University of Science and Technology, Harbin 150080, China; hitrongqin@126.com (Q.R.); 15543095806@126.com (Z.J.)

² Key Lab of Structures Dynamic Behavior and Control of the Ministry of Education, Harbin Institute of Technology, Harbin 150090, China

* Correspondence: nlzzh0920@163.com (Z.Z.); xmhou@hit.edu.cn (X.H.); Tel.: +86-137-9662-7287 (X.H.)

Abstract: Reactive power concrete (RPC) possesses high compressive strength, toughness, and durability, and it is increasingly being used in important buildings. The column is an important load-bearing member of a building, and its failure under blast loading results in building collapse. Based on these attributes, the dynamic response and the degree of damage to the RPC column are critical in assessing building performance. Due to the lack of methods, the progress of the study is relatively slow. In order to solve these issues, the dynamic response of the RPC column is studied based on the equivalent single-degree-of-freedom method and P-I curve in this paper. During the model validation phase, the deformation of the RPC column predicted using the ESDOF approach correlates well with the explosion simulation and test results. The P-I curves of the typical RPC column were also determined, and some data were analyzed to evaluate the influence of different key parameters, such as slenderness ratio, cross-sectional dimension, and axial compression ratio. The results show that the RPC column is susceptible to shear, bending, and bending-shear failure in the impulse load region, quasi-static load region, and dynamic load region, respectively. The cross-sectional dimension and slenderness ratio exhibit the greatest influence on P-I curves among the five parameters. With the increasing cross-sectional dimension and slenderness ratio, the overpressure asymptote of bending response increases by 4.2 times and decreases by about 57.3%. Furthermore, combined with the P-I curve features, it is found that reasonably increasing the cross-sectional dimensions and RPC strength could simultaneously improve the comprehensive anti-blast performance of RPC columns. This study was carried out to obtain the effect of the five parameters mentioned above on the degree of damage under different blast loading, which can provide a valuable reference for the dynamic response of RPC columns.

Keywords: blast loading; reactive powder concrete (RPC); P-I curve; equivalent single-degree-of-freedom (ESDOF); numerical simulation



Citation: Rong, Q.; Zhao, Z.; Hou, X.; Jiang, Z. A P-I Diagram Approach for Predicting Dynamic Response and Damage Assessment of Reactive Power Concrete Columns Subjected to Blast Loading. *Buildings* **2022**, *12*, 462. <https://doi.org/10.3390/buildings12040462>

Academic Editor: Elena Ferretti

Received: 2 March 2022

Accepted: 6 April 2022

Published: 8 April 2022

Publisher's Note: MDPI stays neutral with regard to jurisdictional claims in published maps and institutional affiliations.



Copyright: © 2022 by the authors. Licensee MDPI, Basel, Switzerland. This article is an open access article distributed under the terms and conditions of the Creative Commons Attribution (CC BY) license (<https://creativecommons.org/licenses/by/4.0/>).

1. Introduction

During the last few decades, many explosions worldwide have posed a serious threat to public safety and building structures. Thus, protecting buildings and occupants' lives, while satisfying societal development needs in the future has become of paramount importance. RPC structures have started getting focus and significant attention from scientists and civil engineering experts. The use and research of RPC are increasing day by day in important buildings. Moreover, the column is an important vertical load-bearing component. Its destruction under the blast loading destroys the superstructure, and may even lead to the progressive collapse of the entire building [1]. Therefore, the RPC column may bring some changes in research. It is imperative to study the dynamic response of the RPC column under blast loading.

Scientists across the globe have conducted extensive research on the dynamic behavior of RPC materials and components lately and achieved valuable results. Cao et al. [2] investigated the RPC dynamic compression model, and a dynamic compression model of RPC at elevated temperature was proposed. Yi et al. [3] studied the blast resistance of ultra-high-strength concrete (UHSC) and RPC. The results show that the splitting tensile strength of RPC was higher than that of UHSC, and excellent energy absorption was obtained in short steel fibers RPC. For better analysis of the impact resistance of the materials, the Split Hopkinson Pressure Bar (SHPB) is often used to study the dynamic response. Hou et al. [4] used SHPB to test three kinds of steel fiber RPC (SFRPC) with 0%, 2%, and 5% steel fibers and found that with increasing content of steel fiber, the energy absorption of RPC increased. Wang et al. [5] used SHPB to study the influence of different steel fiber amounts in two-pulse sections of different thicknesses with dynamic strength and failure mode. It was demonstrated that the compressive strength of the RPC is related to the hydrostatic pressure. Wu et al. [6] used SHPB to detect the dynamic differences between pure UHPC and two reinforced UHPC fibers (1.5% and 2%) under three different velocities. Results showed that the fibers can restrict the crack development under dynamic loading. Ren et al. [7] used SHPB ($\varnothing 74$ mm) to perform dynamic compression and tensile tests on steel fiber RPC. It was shown that the dynamic compressive strength of RPC was increased with an increased strain rate. Jiao et al. [8] examined the stress and strain, elastic modulus, strain rate sensitivity threshold, and damage mode of RPC with volume fractions of 0%, 3%, and 4% under impact load. The results found that the strain rate threshold of the material is 30^{-1} . Ju et al. [9] used SHPB to analyze the stress transfer, failure rate, and energy dissipation characteristics of RPC with different fiber volumes and impact speeds. The general shape of the RPC stress-strain state was also determined.

Further, the blast resistance of RPC members has been studied. Fujikake et al. [10,11] studied the impact response of RPC beams by drop hammer impact tests and static bending load tests. It was shown that the maximum mid-span deflection of the RPC beam increases proportionally as the height decreases. Kou et al. [12] analyzed the impact resistance of three RPC and RC panels and found that the impact resistance of the RPC panels was significantly higher than that of the RC panels. Hou et al. [13] combined numerical simulations and experimental control to create a method for estimating the dynamic response and damage of the steel fiber RPC slabs under blast loading. Li et al. [14] used the overpressure-impulse (P-I) to study the damage response of RPC unidirectional slabs under blast loading and analyze the effect of slab width, load level, reinforcement rate, and RPC strength on the shape of the P-I curve and the asymptote.

Many researchers have extensively studied the theoretical calculation methods and dynamic performance of RPC materials, beams, slabs, and other components. Valuable results and findings have been obtained through these studies. However, due to the special behavior of columns in the load-bearing system of building structures, there are few reports on RPC columns, especially on the damage modes and assessment methods of RPC columns under dynamic loading. There is a large discrepancy between the dynamic response and damage assessment of RPC columns in terms of ease and accuracy.

Relevant researchers have carried out some tentative studies on the anti-blast performance of ultra-high-strength concrete columns (UHPC). Li et al. [15] studied the field blasting test of the UHPC column formulated based on RPC. The static axial load test was also carried out on the post-explosion of the UHPC column and the damage degree of the column was analyzed by the P-I curve. However, the P-I curve was calculated based on reinforced concrete columns' P-I curve formula by changing the concrete strength to UHPC strength directly. Due to the dynamic increase factor (DIF) of RPC being smaller than concrete, the calculated P-I curve in [15] will cause an unsafe result. Viet-Chinh Mai et al. [16] used the ABAQUS to explore the dynamic response of UHPC column under explosion load. The influence of key parameters was analyzed, and finally, the P-I curve of the UHPC column according to the maximum loading capacity and residual loading

capacity was calculated. However, the UHPC strength is not considered in the calculation of the P-I curve.

Previous research presented some useful information, but some important factors were not considered. The damage assessment P-I curve of the structure in the literature [15,16] needs to first determine the maximum loading capacity of the column and the residual loading capacity of the column after explosion through the test or simulation software, and then calculate the damage degree. This process increases the computing cycle. Therefore, a handy and accurate method is needed to determine the damage pattern and degree of damage to RPC columns. Currently, the ESDOF method can solve this problem well. In practical engineering, it is necessary to evaluate the peak response of the structure. Under the premise of ensuring accuracy, the difficulty and time of the calculation can be reduced.

In order to improve the problem and try the new research methods, this article presents the P-I diagram method to predict failure modes of RPC columns subjected to blast loading. The criteria and methods based on ESDOF to distinguish damage classification were proposed. A shear fracture criterion is introduced to the failure modes' P-I diagram of columns. The dynamic direct shear model of RPC proposed is utilized. Further, the effects of cross-sectional dimension, RPC strength, longitudinal reinforcement ratio, slenderness ratio, and axial compression ratio on the shape and asymptote were determined. P-I diagrams are handy for the assessment of RPC columns, which can provide a valuable reference for improving the dynamic performance of RPC columns.

2. Dynamic Response of RPC Columns Based on Equivalent Single-Degree-of-Freedom (ESDOF)

2.1. Equivalent Single-Degree-of-Freedom (ESDOF) System

The Equivalent Single-Degree-of-Freedom (ESDOF) method is commonly used to investigate the structurally relevant characteristics under dynamic loading [17–20]. For the convenience of calculation and illustration, a simplified equivalent single-degree-of-freedom system of the RPC column is studied and shown in Figure 1, where the two parts, bending equivalent and shear equivalent components, are included. This study will consider both bending and shear damage effects on RPC columns.

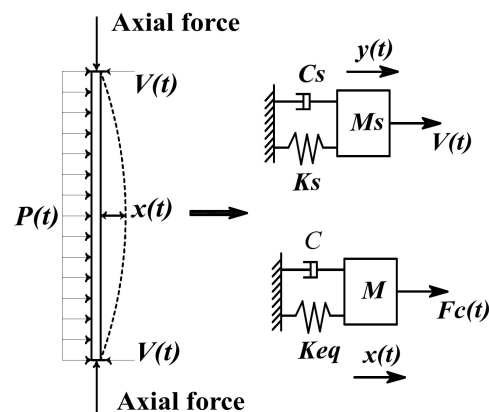


Figure 1. Bending-shear equivalent single-degree-of-freedom system.

The ESDOF method considers a structural unit of uniform mass and external load as a spring-mass ESDOF system. The equivalent mass, resistance, and load [21] values were inserted into the key system equations of motion for calculation. The specific situation is shown in Equation (1).

$$K_M M \ddot{x}(t) + K_L C \dot{x}(t) + K_L R(x) = K_L F_c(t) \quad (1)$$

Equation (1) can also be rewritten as Equation (2).

$$K_{LM}M\ddot{x}(t) + C\dot{x}(t) + R(x) = F_c(t) \quad (2)$$

where M is the total mass of the column; C is the bending viscous damping factor of the column, $R(x)$ is the resistance function; $F_c(t)$ is the external load on the column; K_L is the equivalent load factor; K_M is the equivalent mass factor; K_{LM} is the load-mass factor and $K_{LM} = K_M/K_L$.

Further, the shear ESDOF equation of motion is given as Equation (3).

$$M_s\ddot{y}(t) + C_s\dot{y}(t) + R_s = V(t) \quad (3)$$

where M_s is the shear mass of the column; $y(t)$, $\dot{y}(t)$, and $\ddot{y}(t)$ are the deformation, velocity, and acceleration of shear slip at support, respectively; C_s is the shear viscous damping coefficient of the column; R_s is the shear resistance function; $V(t)$ is the dynamic shear force at support.

2.2. Resistance Functions

Due to the special attributes of this study compared with other research, the effects of both bending and shear damage are considered. So, the resistance function of the RPC column should be divided into two parts, including the equivalent bending resistance function and the shear resistance function.

2.2.1. Bending Resistance Functions

After an extensive review of the relevant literature, the axial compression ratio (the ratio of the applied load (permanent load + variable load) to the column's axial compressive capacity) is considered in the bending resistance function for RPC columns [22]. The following basic assumptions were made for the column [23].

- (1) It does not consider the column initial defect influence;
- (2) The column does not occur instability damage;
- (3) The axial compressive load P has no eccentricity, i.e.,

$$P = uN \quad (4)$$

where N is the axial load capacity; u is the axial compression ratio of the column.

In addition, the ESDOF model has to satisfy the following two basic assumptions [24–27] (the bending resistance functions in the programs also use this model data for computational analysis):

- (1) The whole component should be assumed to be an ideal rigid-plastic unit, and the effects of shear deformation can be ignored when considering the bending deformations.
- (2) The equivalent plastic moment exists at both ends of the column and span. When bending damage occurs to the structure, the ideal plastic hinge appears both at the support and span.

The bending resistance function of the RPC column shows a highly non-linear tendency, and in this study, the bi-fold resistance function model derived from paper [22] is used. The equivalent maximum resistance is \bar{R}_m , as shown in Figure 2.

In Figure 2, R_m is the maximum bending resistance, kN; P is the axial compressive load, kN; Z_E is the maximum elastic displacement, mm; Z_m is the maximum ultimate displacement of the system, mm; L is the height of the column, m.

After calculation and derivation, it was found that the stiffness and resistance of the system decreased to a certain extent after the addition of external axial compressive load. The resistance function in the final derivation is expressed with the equivalent maximum resistance and the equivalent joint stiffness.

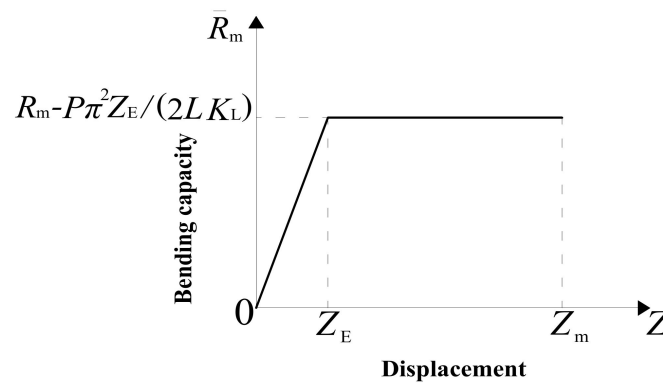


Figure 2. Bending resistance function.

This paper has a large number of derivation parameters, the specific parameter calculation methods can be found in the reference [22], and the results are shown in Table 1. Finally, the characteristic parameters of the ESDOF system, considering the effect of the axial compression ratio, can be obtained by using Equation (4) in Table 1. This Equation can be reduced to the conventionally ESDOF system when the axial compression ratio is zero.

Table 1. Model characteristics parameters.

Transformation Phase	Load Factor K_L	Quality Factor K_M	Load Mass Factor K_{LM}	Equivalent Maximum Resistance $\bar{R}_m = R_m - \frac{k_G^*}{K_L} Z_E$		Equivalent Joint Stiffness $\bar{k}_e = k - \frac{k_G^*}{K_L}$	
				Maximum Bending Resistance R_m	Maximum Geometric Resistance $\frac{k_G^*}{K_L} Z_E$	Bending Stiffness k	Geometric Stiffness $\frac{k_G^*}{K_L}$
Elastic	0.64	0.50	0.76			$\frac{307EI}{L^3}$	$\frac{\lambda N \pi^2}{2LK_L}$
Elastic-Plastic	0.64	0.50	0.78	$\frac{8}{L} (M_{ps} + M_{pm})$	$\frac{\lambda N \pi^2}{2LK_L} Z_E$		
Plastic	0.50	0.33	0.66			0	$\frac{4\lambda N}{LK_L}$

Note: M_{ps} is the column span bending moment, and M_{pm} is the column support bending moment.

2.2.2. Shear Resistance Functions

Although the current study does not precisely define the shear resistance function for RPC columns, an analogous study based on other models also could be recognized. For the shear resistance function of the RPC column, the direct shear model of concrete [28] is used. Meanwhile, some data for RPC mechanical properties in this study will be redefined based on the reference [28]. The specific form of the shear resistance function is shown in Figure 3.

As shown in Figure 3, the slips corresponding to points A, B, C, and D are Δ_1 , Δ_2 , Δ_3 , and Δ_{max} . The shear strengths corresponding to points A and C are the maximum shear strength τ_{max} , and the residual shear strength τ_L . Moreover, the slope K_1 of the OA segment represents the slope of the model strength after cracking, and the slope K_u of the BC segment represents the slope of the shear strength after exceeding the maximum value.

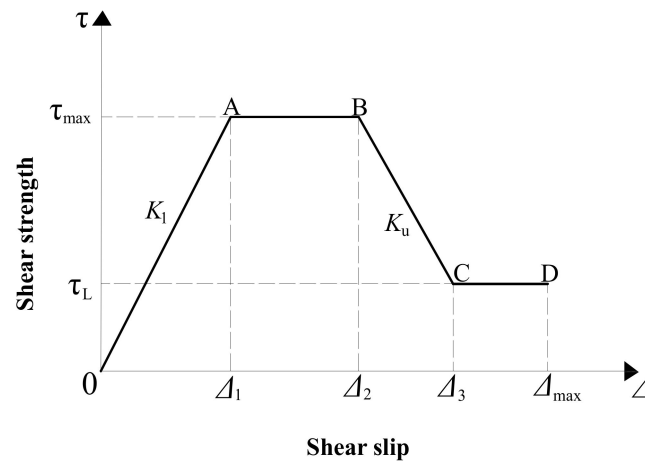


Figure 3. Shear resistance functions.

2.3. Dynamic Increase Factor

Dynamic increase factor (*DIF*) is a ratio of dynamic to static strength with strain rate under dynamic loading. Compared with static loading effects, the most obvious phenomenon is the increase in dynamic strength at high strain rates. The formula for determining *DIF* is given as Equation (5).

$$DIF = \sigma_d / \sigma_s \quad (5)$$

In this study, the *DIF* of RPC and steel reinforcement was used in [13,29], respectively, as shown in Equations (6) and (7).

$$DIF_{RPC} = \sigma_d / \sigma_s = a(\dot{\epsilon})^{0.5} 70s^{-1} \leq \dot{\epsilon} \leq 320s^{-1} \quad (6)$$

where σ_d and σ_s are the dynamic and static stresses in the RPC respectively; $a = 10^{9.621\alpha - 1.092}$; $\alpha = (f_{cu} - 50.65)^{-1}$; f_{cu} is the compressive strength of the RPC cube.

$$DIF_{steel} = f_{yd} / f_{ys} = \left(\dot{\epsilon} / 10^{-4} \right)^{(0.074 - 0.04f_y / 414)} \quad (7)$$

where $\dot{\epsilon}$ is the strain rate of the steel bar; f_{yd} and f_{ys} represent the dynamic yield strength and static yield strength of the steel, respectively; f_{yd} / f_{ys} is the dynamic growth factor of the yield strength of the steel bar.

2.4. Experimental and Numerical Calculation Model Validation

In order to corroborate the validity and accuracy of the ESDOF computational analysis procedure, the comparative verification of the ESDOF method by experiments and numerical calculation model is presented in this section.

2.4.1. Experimental Validation

The experimental results [30] were selected to contrast with the results of the SDOF numerical calculations. In the experiment, the overall dimension of the ultra-high performance concrete (UHPC) column is 200 mm × 200 mm × 2500 mm, and the diameter of longitudinal reinforcement and stirrup reinforcement is 16 mm and 8 mm, respectively. Besides, for the mechanical properties of materials, the longitudinal bearing reinforcement yield strength adopts 435 MPa, and the compressive strength of the UHPC adopts 148 MPa. Detailed dimensions of the UHPC column and reinforcement in the test are shown in Figure 4. The test blast working conditions are shown in Table 2.

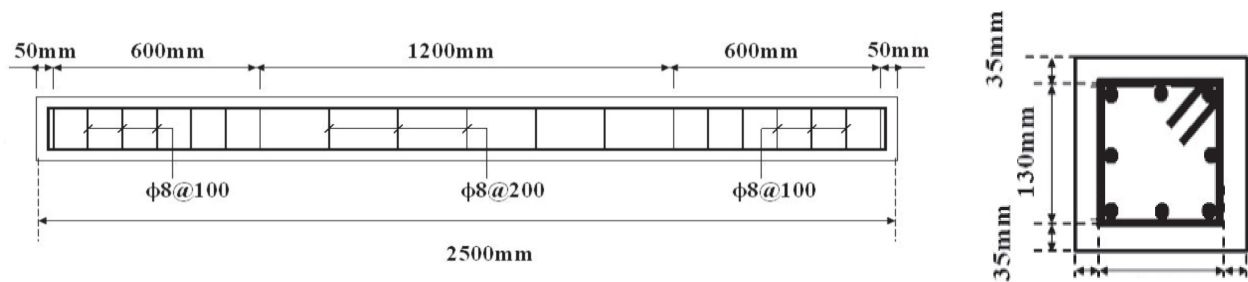


Figure 4. The sectional size of UHPC column and reinforcement.

Table 2. Different explosion conditions.

Working Condition	Amount of Explosives/kg	Blast Distance/m	Scale Distance/m/kg ^{1/3}	Pressure/MPa	Impulse/MPa	Time/ms
1	8	1.5	0.75	28.68	6.37	0.44
2	17.5	1.5	0.58	64.88	13.76	0.42

The experimental time–displacement curves [30] that only select the part with its displacement and neglect the smoothing section were extracted and compared with the results of ESDOF calculations in this study. The specific comparison curves are shown in Figure 5.

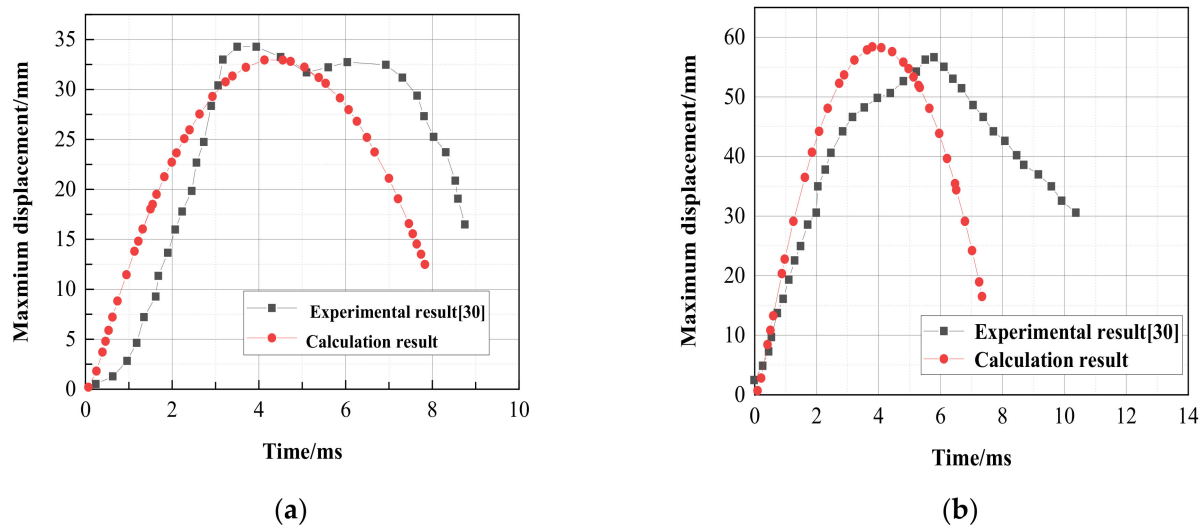


Figure 5. Comparison between the experimental results and ESDOF calculation results. (a) Comparison of time–displacement curves for working condition 1. (b) Comparison of time–displacement curves for working condition 2.

2.4.2. Numerical Calculation Model Validation

The numerical calculation model is also studied. The validation calculation model is selected from the column calculation analysis results [31] for SDOF model checking. The overall column dimension is 406 mm × 406 mm × 3660 mm. The diameters of longitudinal reinforcement and stirrup diameter adopt 22 mm and 10 mm, respectively. The longitudinal bearing reinforcement yield strength is 475.7 MPa, while the ultimate yield strength is 751.5 MPa. Additionally, RPC strength is designed as 140 MPa. The blast load conditions are shown in Table 3.

Table 3. Different blast load conditions.

Working Conditions	Explosive Overpressure/MPa	Explosive Impulse/MPa ms	Duration of Action/ms
C1-Medium to high strength	20.15	12.93	1.28
C2-Medium to low strength	8.16	5.40	1.32
C3-low strength	4.25	3.16	1.49

The analysis results [31] were also extracted and compared with the results of the SDOF calculations in this study. The comparison results of the specific mid-span maximum displacement time curves are shown in Figure 6.

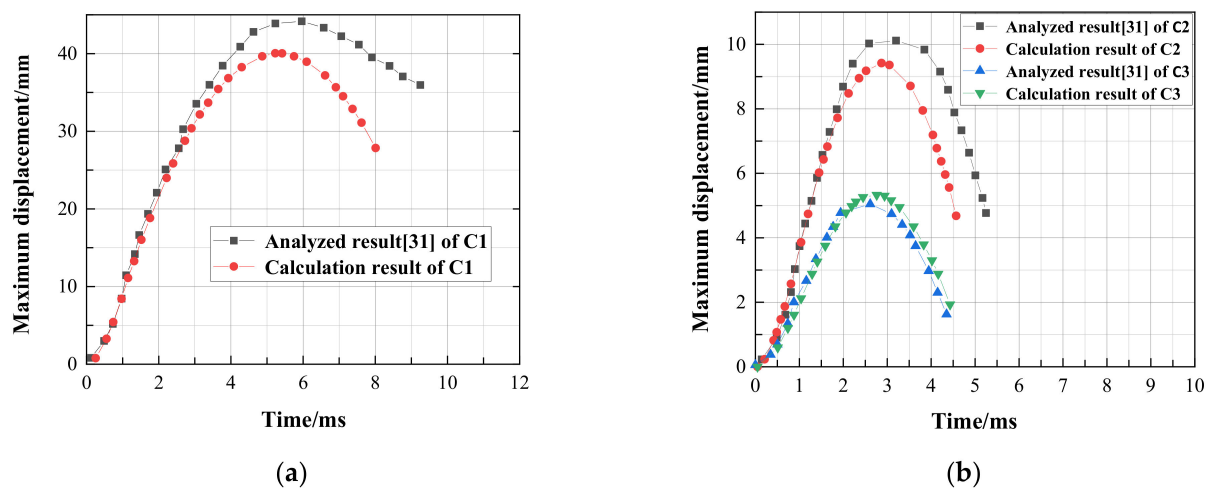


Figure 6. Comparison between the simulation calculation and ESDOF calculation result. (a) Comparison of time–displacement curves for C1. (b) Comparison of time–displacement curves for C2 and C3.

The discrepancies in the validation results shown in Figures 5 and 6 are mainly because the RPC column was not uniformly distributed in the internal material during fabrication. RPC may respond at their local modes under blast loading, while the ESDOF system using the fundamental response mode might not be perfectly suitable. In addition, the ESDOF approach has difficulties in predicting the local failure modes of columns. However, it can be concluded from Figures 5 and 6 that the ESDOF method can predict the deformation of RPC columns under blast loading accurately.

2.5. Criteria for Judgment of Damage

2.5.1. Bending Damage Criteria

Bending damage has been addressed in many investigations and studied as the main damage mode in civil engineering. Nevertheless, for practical blast assessment and research, the degree of damage at the mid-span is commonly used to determine the degree of damage to the components. Thus, the maximum rotating angle of the column end, θ_{\max} , is used to determine the degree of damage. θ_{\max} can be converted into the maximum mid-span displacement, Δ_{\max} . The specific definition is shown in Figure 7, and the formulas are given as Equations (8) and (9).

$$\theta_{\max} = \arctan\left(\frac{2\Delta_{\max}}{H}\right) \frac{180}{\pi} \quad (8)$$

$$\Delta_{\max} = \frac{\pi}{180} \frac{2\tan(\theta_{\max})}{H} \quad (9)$$

where θ_{\max} is the maximum rotating angle; Δ_{\max} is the maximum central displacement of columns; H is the column height.

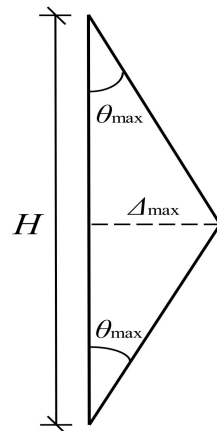


Figure 7. Diagram of the maximum rotating angle at column end.

Three bending damage criteria are selected from the paper [32]. However, these should be converted and combined with Equations (8) and (9) for the maximum displacement at mid-span and the rotating angle at the column end. The parameter, $2\Delta_{\max}/H$, is converted to the parameter, θ_{\max} . The damage criteria defined in this section will be used to calculate the P-I curve in Section 4. The specific bending damage criteria are shown in Table 4.

Table 4. Bending damage criteria.

Damage Level	Light Damage	Medium Damage	Serious Damage
Ratio of deformation to column half-span length, $2\Delta_{\max}/H$ [32]	2%	6%	12.5%
The maximum rotating angle at column end, θ_{\max}	1.4°	3.4°	7.1°

Note: Δ_{\max} in Figure 7 and Table 4 represents the maximum deformation in the column; H represents the column height; $2\Delta_{\max}/H$ values are given as percentages in Table 4.

2.5.2. Shear Damage Criteria

Since shear damage has rarely been considered in previous studies, there is no valid standard for defining the criteria. Therefore, the shear damage criteria are selected directly from reference [13]. The average shear strain γ at the bearing is used to determine the degree of shear damage, as shown in Table 5.

Table 5. Shear damage criteria.

Damage Degree	Light Damage	Medium Damage	Serious Damage
Average shear strain/ γ	1%	2%	3%

The average shear strain at the bearing can be calculated using Equations (10) and (11) [33,34].

$$\gamma_s = \gamma e \rightarrow \gamma = \gamma_s / e \times 100\% \quad (10)$$

$$e = \sqrt{3}B/8 \quad (11)$$

where γ_s is the accumulated shear slip magnitude in the shear deformation zone, γ is the average shear strain in the shear deformation zone, e is the half-width of the shear deformation zone of the member and B is the height of the column cross-section.

The bending and shear damage discrimination criteria are defined, respectively. Each criterion has three levels—light damage, medium damage, and serious damage. While analyzing the degree of damage under blast loading and calculating bending-shear coupled P-I curves, the damage discrimination criteria are used and defined in Table 6.

Table 6. Criteria of bending and shear damage.

Damage Category	Judgment Parameters	Light Damage	Medium Damage	Serious Damage
Bending damage	Maximum rotating angle at column end [θ]	1.4°	3.4°	7.1°
Shear damage	Average shear strain [γ]	1%	2%	3%

3. P-I Curve

P-I curve was first introduced in the Second World War to assess the damage degree of buildings under blast loadings. Subsequently, it was also refined to assess the damage to occupants and structures by experts and academics. Its basic form is shown in the paper [35]. From left to right and top to bottom in the same curve could be divided into three parts. i.e., the impulsive load region, dynamic load region, and quasi-static load region.

P-I curve methods for predicting the intensity of RPC column damage can also be divided into three main steps as follows.

First step: Input calculation parameters and establish criteria

- (1) Inputting model parameters such as column height, cross-sectional dimension, RPC strength, and longitudinal reinforcement rate et al. into the calculation program.
- (2) Designing the explosive charge and blast distance, and calculating the overpressure and duration of the blast, the moment of inertia of the RPC column, stiffness, and other parameters.
- (3) Establishing the bending-shear failure criteria of the RPC column.

Second step: Calculate the program and output the resulting curve

- (1) Using the *Newmark- β* method to solve the bending-shear ESDOF equations of motion, the RPC column bending and shear displacement time curves can be obtained. The maximum displacement value also can be obtained.
- (2) Obtaining the amount of explosive charge corresponding to the maximum displacement of the target, the blast distance, and the overpressure-impulse (P-I) value.

Last step: Plot the P-I curves

- (1) The P-I value corresponding to the maximum displacement is recorded, and the corresponding point is plotted.
- (2) Changing the blast condition and repeating the above process to obtain a complete P-I curve plot to predict the failure mode of the RPC column based on a specific parameter.

To facilitate the reader's understanding of the P-I graph plotting process, Figure 8 depicts the process of obtaining a complete P-I curve.

After calculating the values of the P-I corresponding to the blast loading, it is necessary to use the P-I curve to determine the classification and degree of damage under blast loading. The following section will define the typical RPC column parameters and calculate a typical RPC column bending-shear P-I curve. This step aims to reveal how to distinguish the classification and degree of damage to the structural components.

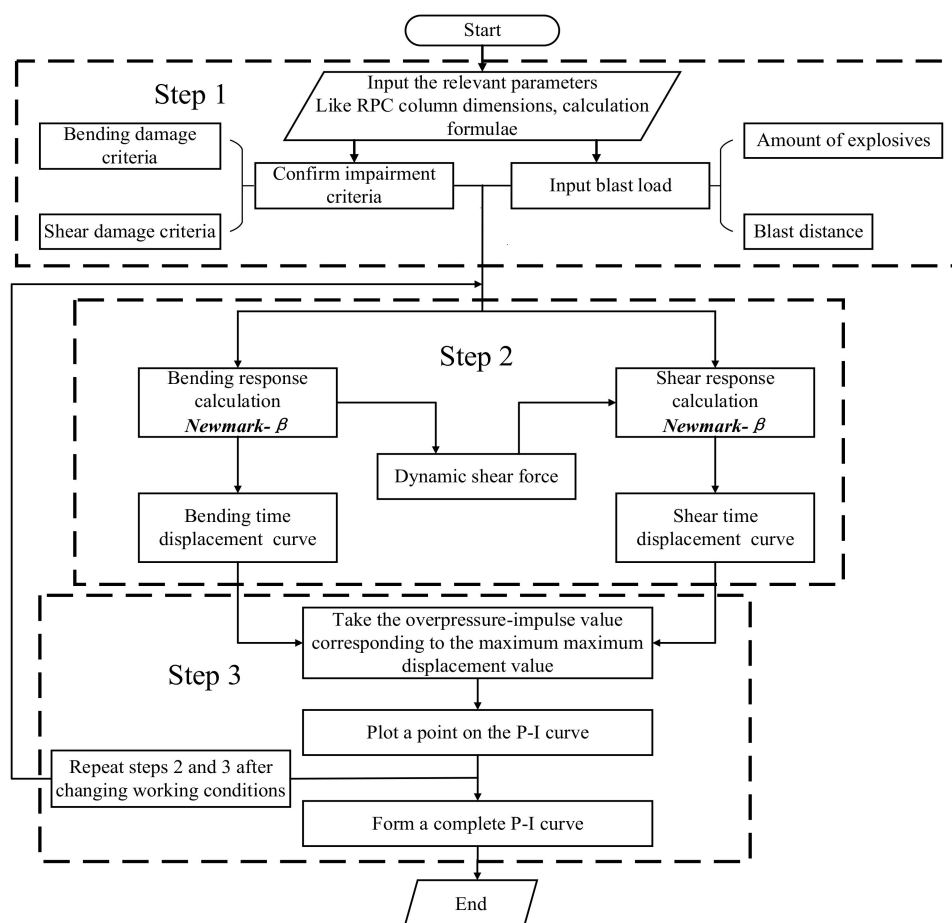


Figure 8. Flow chart for calculation of RPC columns P-I curves.

P-I Curve of Typical RPC Column

To pave the way for the parametric analysis in the next section, the parameters of the typical RPC column and its P-I curve are designed and calculated in this section. To make the numerical calculation results more evidence-based, the component dimension and internal reinforcement materials involved in this study refer to the material data of the test members in the paper [14]. The specific parameters are shown in Table 7. The P-I curves are shown in Figures 9 and 10.

Table 7. Calculation parameters of typical RPC column.

Basic Material Parameters	
Cross-sectional dimension $L \times B \times H$ /mm	400 × 400 × 2500
Compressive strength of RPC/MPa	100
Tensile strength of RPC/MPa	6.86
Modulus of elasticity of RPC/ 10^4 MPa	3.79
Tensile strength of HRB500 reinforcement/MPa	435
Diameter of longitudinal reinforcement/mm	16
Hoop diameters/mm	8

As shown in Figure 10, the four curves can be seen. Within the four curves, ① and ② represent light and serious bending damage curves, whereas ③ and ④ represent light and serious shear damage curves. Four curves divide the diagram into six major segments, i.e., A, B, C, D, E, and F.

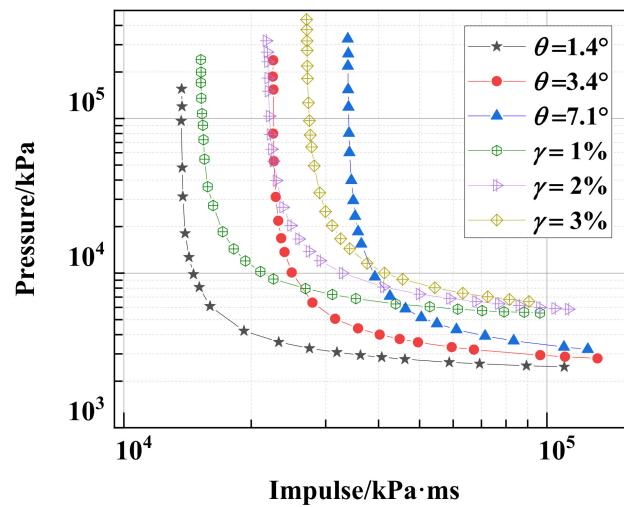


Figure 9. Bending-shear response P-I curves.

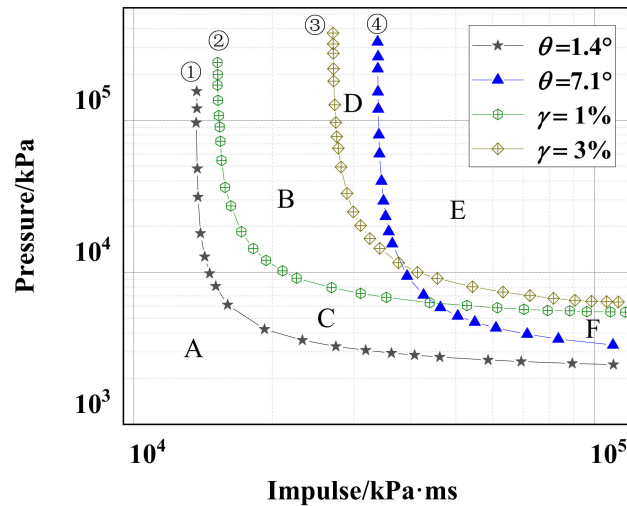


Figure 10. Divisions of bending-shear response P-I curve.

Each curve represents the critical value of the degree of damage. The points on either side of the curve represent the degree of completely different damage. For example, the points in region C have exceeded the lower limit of bending light damage, but not the lower limit of light shear damage. Therefore, C can be judged as a light-bending damage region. Similarly, F can be identified as a serious bending damage region. B can be judged as a light shear damage region. A and D are safe and serious shear damage regions, respectively. However, for region E, this scenario needs to be further divided into two cases based on the damage to the column support:

- (1) If the column has reached shear failure before bending failure occurs, the column will have only shear failure;
- (2) If the shear failure does not occur before bending damage, the column will have bending-shear failure.

In general, when the corresponding overpressure-impulse point is located on the curve, the damage to the structure is considered to be higher, which is the basic principle of the P-I curve assessment.

4. Effect of Parameters for P-I Curve

In order to reveal the influence of RPC column parameters on the shape of the P-I curve and its asymptote, the five key parameters, slenderness ratio, cross-sectional dimension, RPC strength, longitudinal reinforcement ratio, and axial compression ratio governing the dynamic response and failure mode of RPC columns under blast loading are selected. The range of parameters is determined by the basics of common constructions [36,37].

The comparative results of P-I curves and asymptotes under the key parameters are shown in the figures below. Four values in each key parameter are transformed to enhance diversity and reliability. In the following analysis of the P-I curve parameters, the curves corresponding to the smallest degree of damage in the bending-shear response P-I curves (bending damage, 1.4°; shear damage, 1%) are utilized in the quantitative analysis since every figure has a large number of curves.

4.1. Slenderness Ratio

In order to study the influence of the slenderness ratio of the RPC column on the P-I curve and asymptote, it is combined with the limited range of slenderness ratio λ according to the guidelines of the “Code for the design of concrete structures” (GB50010-2010) [38]. From the above code, it can be found that the λ value of the square column should be between 8 and 28. In this section, the P-I curves of the five RPC columns, slenderness ratios are 8.66, 10.83, 12.99, 15.16, and 17.32, respectively, are investigated.

As shown in Figure 11, with the increasing slenderness ratio, the P-I curves move down and left. Since the column changes from a short column to a slender column, the moment of inertia and stiffness of the cross-section are greatly reduced, and the flexural and shear capacity of the RPC column are reduced simultaneously. This change can make the RPC column prone to damage under dynamic loading. In addition, as the slenderness ratio increases, the shape of the bending response changes significantly.

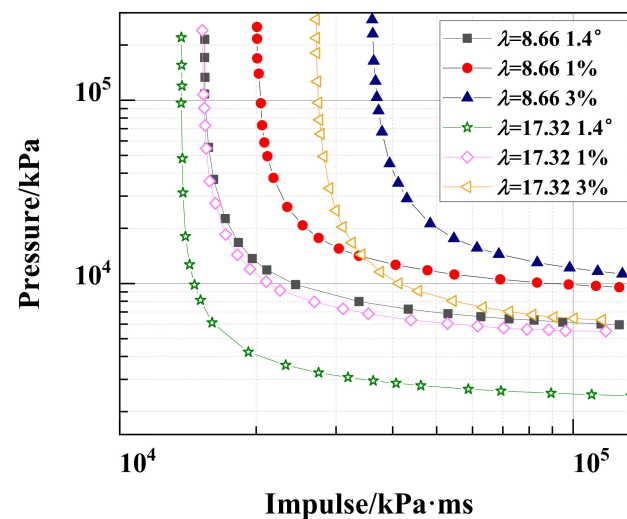


Figure 11. Analysis of P-I curves with two slenderness ratios, 8.66 and 17.32.

As shown in Figures 12 and 13, the shape of P-I curves for bending response changes significantly, and the impulse asymptote becomes closer. Table 8 shows the regulation of overpressure-impulse asymptote in two classifications of damage. The results show that with the increasing slenderness ratio, the overpressure-impulse asymptote of bending response decreases by about 57.3% and 10.2%, respectively. The overpressure asymptote of the shear response decreases by about 41.1% and 37.9% as the slenderness ratio increases, and the impulse asymptote decreases about 23.7% and 24.7%.

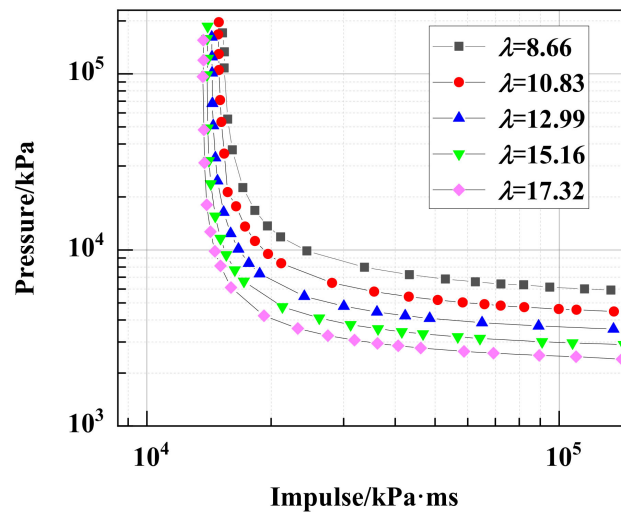


Figure 12. P-I curves of bending response with different slenderness ratios.

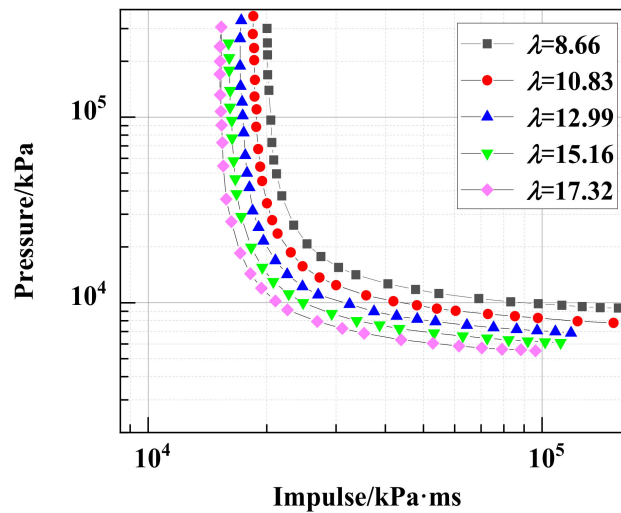


Figure 13. P-I curves of shear response with different slenderness ratios.

Table 8. Effect of slenderness ratios on asymptotes.

Slenderness Ratios/ λ	$\theta = 1.4^\circ$		$\gamma = 1\%$		$\gamma = 3\%$	
	P_0/kPa	$I_0/kPa\ ms$	P_0/kPa	$I_0/kPa\ ms$	P_0/kPa	$I_0/kPa\ ms$
8.66	5791	15,262	9366	19,916	10,544	35,905
10.83	4379	14,944	7597	19,111	8420	34,199
12.99	3556	14,356	6874	17,120	7994	30,220
15.16	2901	13,997	6098	15,995	7084	28,552
17.32	2474	13,701	5514	15,201	6551	27,028

In conclusion, as the slenderness ratio increases, the P-I curve asymptotes of bending-shear response both reduce to varying degrees. However, the overpressure asymptote of bending response is significantly affected. Combined with the characteristics of the P-I curve quasi-static load region, increasing the slenderness ratio may increase the degree of bending damage at mid-span. Reasonably, reducing the slenderness ratio may effectively enhance the bending capacity of the RPC column at mid-span under blast loading.

4.2. Cross-Sectional Dimension

Five cross-sectional dimensions (200×200 mm, 300×300 mm, 400×400 mm, 500×500 mm, and 600×600 mm) of RPC column were selected to investigate its effect on the shape and the asymptote of P-I curves for bending-shear damage.

As shown in Figure 14, as the cross-sectional dimension increases from 200×200 mm to 600×600 mm, the P-I curves of bending-shear response both shift to the upper and right region. That means the overpressure-impulse asymptotes both increase at the same time. This is because the larger cross-sectional dimension results in a greater moment of inertia, which induces superior dynamic load resistance of the RPC column. In addition, with the change in cross-sectional dimension, the shape of the bending response P-I curves changes significantly.

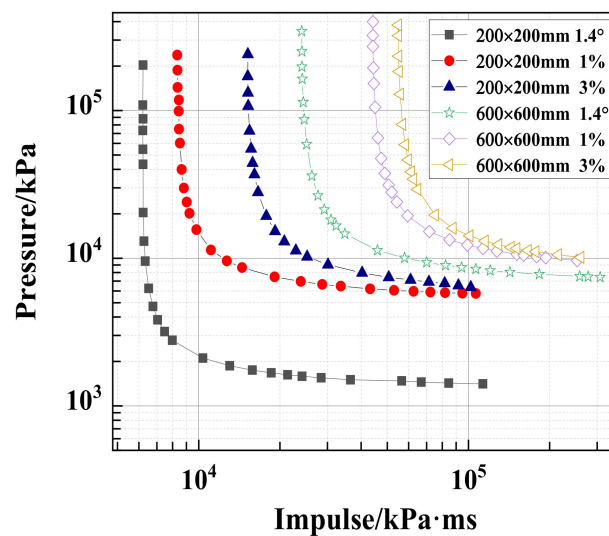


Figure 14. Analysis of P-I curves with cross-sectional dimensions, 200×200 mm and 600×600 mm.

As shown in Figures 15 and 16, the overpressure-impulse asymptote of bending response increases uniformly as the cross-sectional dimensions increase, while the impulse asymptote of shear damage changes more than the overpressure asymptote. Table 9 reveals the regulation of overpressure-impulse asymptotes in two classifications of damage. The results show that as the cross-sectional dimension increases, the overpressure-impulse asymptote of bending response increases by 4.2 and 2.9 times (calculated by columns 2 and 3 in Table 9), respectively. In addition, the overpressure asymptotes of shear response increase by 0.5 and 0.6 times more than before (calculated by columns 4 and 6 in Table 9). The impulse asymptotes increase by 2.64 and 2.6 times, respectively, (calculated by columns 7 and 9 in Table 9).

Table 9. Effect of cross-sectional dimension on asymptotes.

Cross-Section Dimensions/mm ²	$\theta = 1.4^\circ$		$\gamma = 1\%$		$\gamma = 3\%$	
	P_0 /kPa	I_0 /kPa ms	P_0 /kPa	I_0 /kPa ms	P_0 /kPa	I_0 /kPa ms
200×200	1439	6208	5771	8354	6355	15,201
300×300	2984	10,575	6617	12,931	7547	23,093
400×400	4379	14,897	7597	19,111	8420	34,199
500×500	5764	19,307	8381	24,475	9887	43,585
600×600	7438	24,101	8789	30,429	10,139	54,699

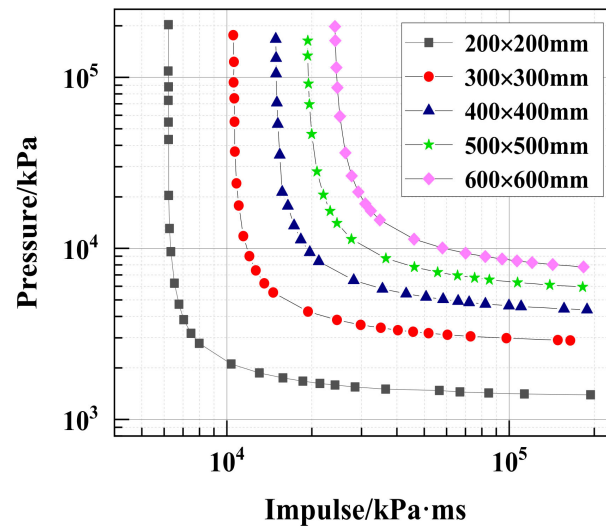


Figure 15. P-I curves of bending response with a different cross-sectional dimension.

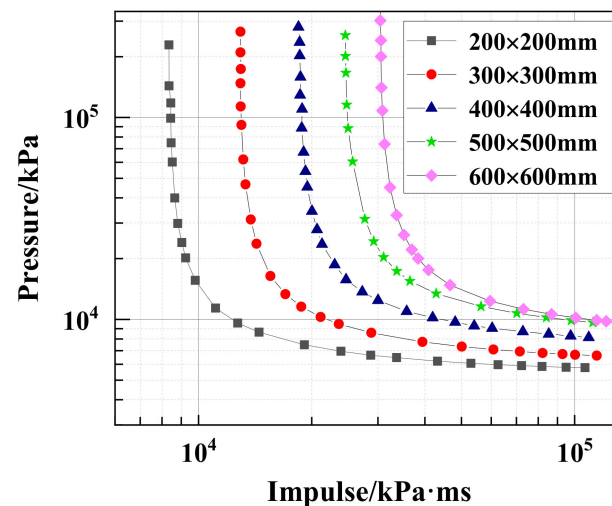


Figure 16. P-I curves of shear response with a different cross-sectional dimension.

In summary, the change in cross-sectional dimensions primarily affects the overpressure asymptote of the bending response. However, for the shear response, the change in the impulse asymptote is much greater than the overpressure asymptote. Combined with the impulse and quasi-static load region characteristics, increasing cross-sectional dimension can effectively improve the bending capacity at mid-span and the shear capacity at support subjected to blast loading. It signifies that increasing the cross-sectional dimension within a reasonable range can significantly enhance the comprehensive anti-blast performance of the RPC column.

4.3. RPC Strength

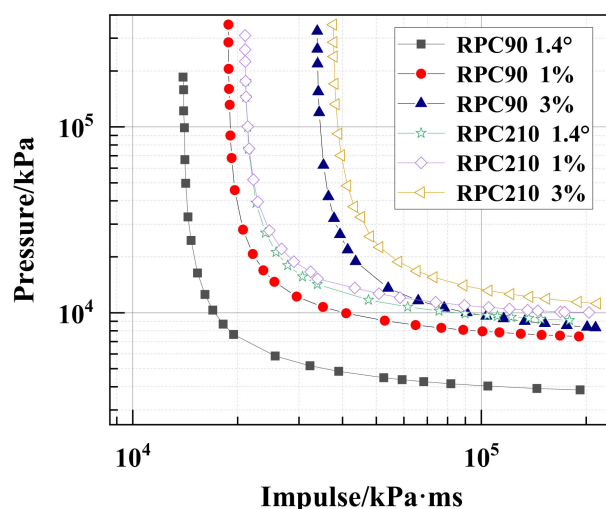
RPC is increasingly used in buildings because of its high strength, toughness, and durability. In this study, numerical simulations are used to investigate the effect of RPC material strength on the shape and the asymptote of the P-I curve for different damage classifications. Five RPC strengths (the standard values of RPC compressive strength), 90 MPa, 100 MPa, 140 MPa, 180 MPa, and 210 MPa, are selected for investigation. Mechanical properties parameter values of RPC have been summarized [39]. The Mechanical properties of RPC in the simulation are listed in Table 10.

Table 10. Mechanical property index for each strength of RPC.

Strength Grade/MPa	Compressive Strength/MPa		Tensile Strength/MPa		Modulus of Elasticity/ 10^4 MPa
	Standard Values	Design Value	Standard Values	Design Value	
RPC90	90	58.9	5.95	4.58	3.60
RPC100	100	65.4	6.86	5.27	3.79
RPC140	140	91.4	10.12	7.79	4.25
RPC180	180	117.5	13.01	10.01	4.70
RPC210	210	136.8	14.93	11.49	4.99

Note: Poisson's ratio is 0.2 for RPC [40].

As shown in Figure 17, it is found that as the RPC strength increases, the P-I curve of bending damage shifts to the upper right area, whereas the P-I curve of shear damage shifts to the lower left. In addition, as the change of RPC strength, P-I curves of bending-shear damage in the quasi-static load region become closer to each other. The curves of the same degree of damage for different RPC strengths in the shear response impulse load region almost overlap. This phenomenon occurs possibly because increasing RPC strength does not, to a certain extent, result in a significant increase in the shear capacity of the column at the supports. However, increasing RPC strength will, to a certain extent, result in brittle damage at support and reduce the shear capacity of the column.

**Figure 17.** Analysis of P-I curves with two RPC strengths, 90 MPa and 210 MPa.

As shown in Figures 18 and 19, with the increase in RPC strength, the changing magnitude of the overpressure-impulse asymptote of the bending response is greater than the shear response. It indicates that increasing RPC strength primarily enhances the bending capacity of the component. Table 11 shows the pattern of overpressure-impulse asymptotes in two damage classifications. The results show that as the RPC strength increases from 90 MPa to 210 MPa, the overpressure-impulse asymptote of bending response increases by 1.32 and 0.51 times more than before (calculated in columns 2 and 3 in Table 11). Further, the overpressure asymptote of shear response increases by 0.35 and 0.34 times (calculated by columns 4 and 6 in Table 11), whereas the impulse asymptote increases by 0.12 and 0.11 times than before (calculated by columns 5 and 7 in Table 11), respectively.

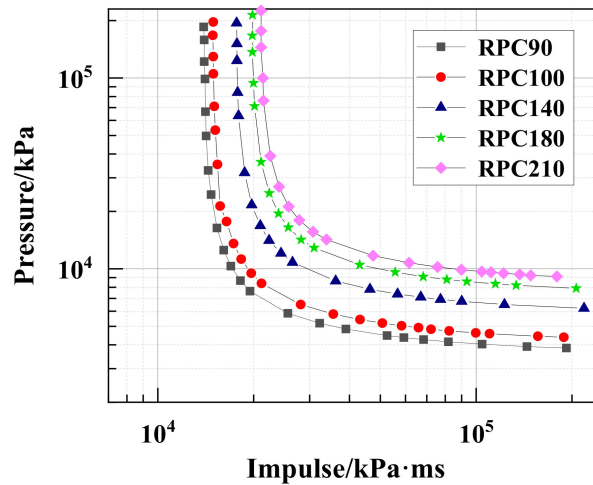


Figure 18. P-I curves of bending damage with different RPC strength.

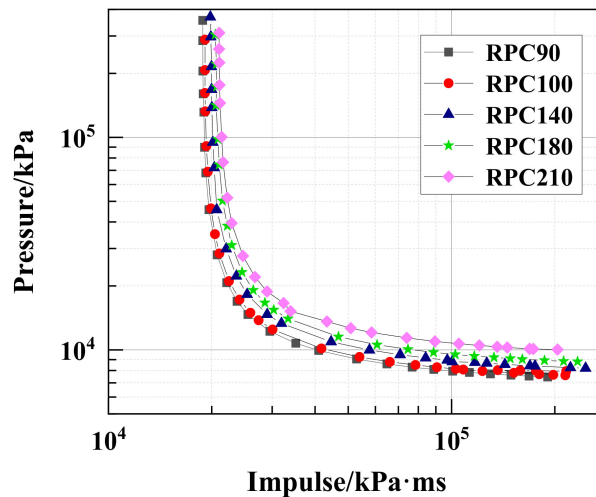


Figure 19. P-I curves of shear damage to different RPC strength.

Table 11. Effects of RPC strength on asymptotes.

RPC Strength/MPa	$\theta = 1.4^\circ$		$\gamma = 1\%$		$\gamma = 3\%$	
	P_0/kPa	$I_0/kPa\ ms$	P_0/kPa	$I_0/kPa\ ms$	P_0/kPa	$I_0/kPa\ ms$
RPC90	3846	13,997	7452	18,824	8314	33,705
RPC100	4379	14,944	7597	19,111	8420	34,199
RPC140	6047	17,692	8203	19,813	9135	35,678
RPC180	7765	19,834	8812	20,492	9744	36,860
RPC210	8907	21,102	10,035	21,005	11,208	37,427

In summary, as the RPC strength increases from 90 MPa to 210 MPa, the overpressure-impulse asymptote of bending response and shear response become larger, but the shear response has a relatively smaller magnitude. Increasing RPC strength mainly affects the overpressure asymptote for P-I curves of bending-shear response. Combined with the features of quasi-static load region, increasing RPC strength, for mid-span or support of RPC column, both could improve the anti-blast performance under the explosion. In other words, the use of higher strength RPC can effectively enhance the comprehensive anti-blast performance of RPC columns.

4.4. Longitudinal Reinforcement Ratio

In order to study the effect of longitudinal reinforcement ratio on P-I curves and asymptotes, according to the “Code for design of concrete structures” (GB50010-2010) [38], five longitudinal reinforcement ratios, 0.77%, 1.01%, 1.3%, 1.6%, and 1.9%, were calculated and analyzed.

As shown in Figure 20, P-I curves of bending-shear damage shift to the upper right region as the longitudinal reinforcement ratio increases from 0.77% to 1.9%. This trend indicates overpressure-impulse asymptotes both increasing. Because changing the number of longitudinal bars and diameters increase the longitudinal reinforcement ratio and increases the number of hoop reinforcement and minimum diameter. These variations increase the bending-shear capacity of the RPC column.

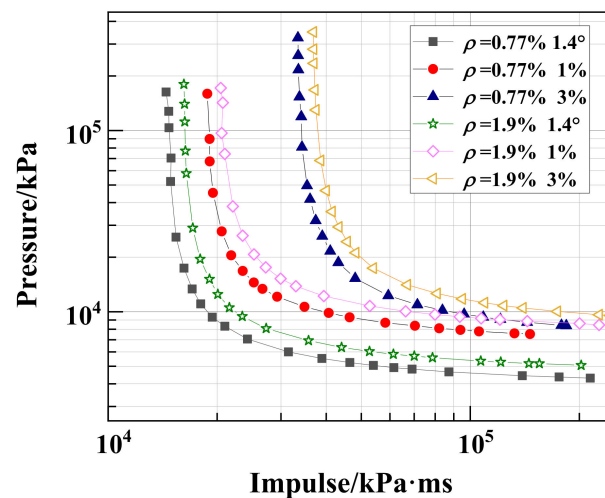


Figure 20. Analysis of P-I curves with two longitudinal reinforcement rates, 0.77% and 1.9%.

As shown in Figures 21 and 22, the increasing longitudinal reinforcement ratio both affects the P-I curve of bending-shear response, but the extent is different. Table 12 reveals the trend of the overpressure-impulse asymptote in two damage classifications. The results show that as the longitudinal reinforcement ratio increases from 0.77% to 1.9%, the overpressure asymptote of bending response increases by about 17.8% (calculated by column 2 in Table 12), while the impulse asymptote increases by about 12% than before (calculated by column 3 in Table 12). However, the overpressure asymptote of shear response increases by about 12.8% and 8.8% (calculated by columns 4 and 6 in Table 12), and the impulse asymptote increases by about 13.8% and 10.3%, respectively, (calculated by columns 5 and 7 in Table 12).

Table 12. Effect of longitudinal reinforcement rate on asymptotes.

Reinforcement Rate/%	$\theta = 1.4^\circ$		$\gamma = 1\%$		$\gamma = 3\%$	
	P_0/kPa	$I_0/\text{kPa ms}$	P_0/kPa	$I_0/\text{kPa ms}$	P_0/kPa	$I_0/\text{kPa ms}$
0.77	4298	14,451	7522	18,788	8375	33,428
1.01	4379	14,897	7597	19,111	8420	34,199
1.3	4413	15,079	7877	19,504	8661	35,171
1.6	4607	15,445	8326	20,032	9172	35,944
1.9	5061	16,184	8457	20,450	8536	36,859

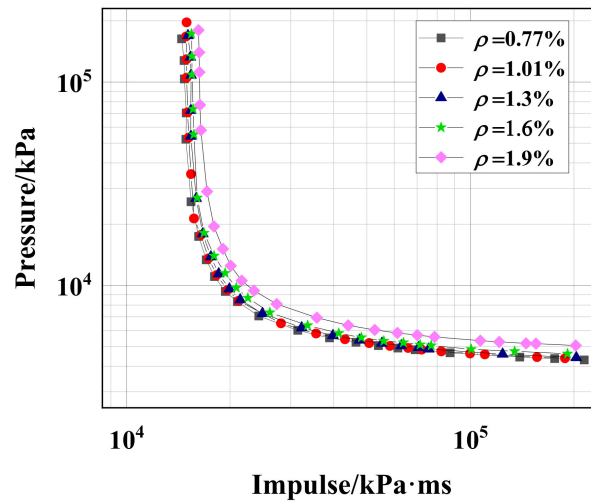


Figure 21. P-I curves of bending response with different longitudinal reinforcement ratios.

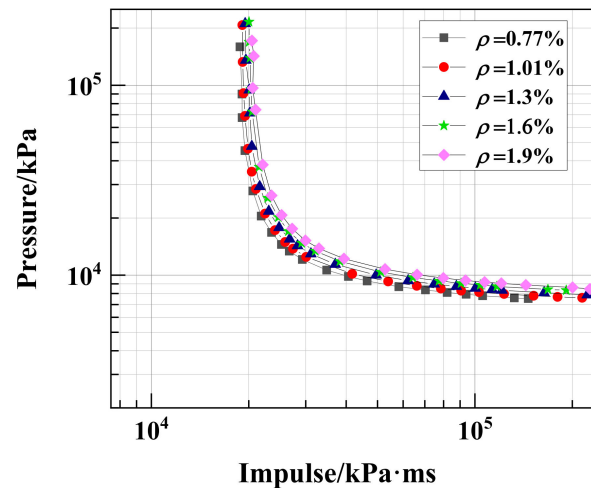


Figure 22. P-I curves of shear response with different longitudinal reinforcement ratios.

In summary, the effect of increasing the longitudinal reinforcement ratio on the bending response is greater than the shear response. The change of longitudinal reinforcement ratio mainly affects the overpressure asymptote. Combined with the characteristics of the quasi-static load region, increasing the longitudinal reinforcement ratio of the RPC column can effectively improve the bending capacity at mid-span under the blast loading. In other words, reasonably increasing the longitudinal reinforcement ratio of RPC columns can resist blast loading at mid-span.

4.5. Axial Compression Ratio

To examine the effect of the axial compression ratio on the shape and the asymptote of the P-I curve, five RPC columns with different axial compression ratios, 0.1, 0.3, 0.5, 0.7, and 0.8, were studied, following the upper limit of column axial compression ratio in the Chinese Code “Seismic design of buildings” (GB50011-2011) [41].

As the axial compression ratio increases in Figure 23, the P-I curve of bending response shifts down and left, but the shear response curve shifts toward up and right. This phenomenon indicates that increasing the axial compression ratio could significantly affect the bending capacity of the RPC column.

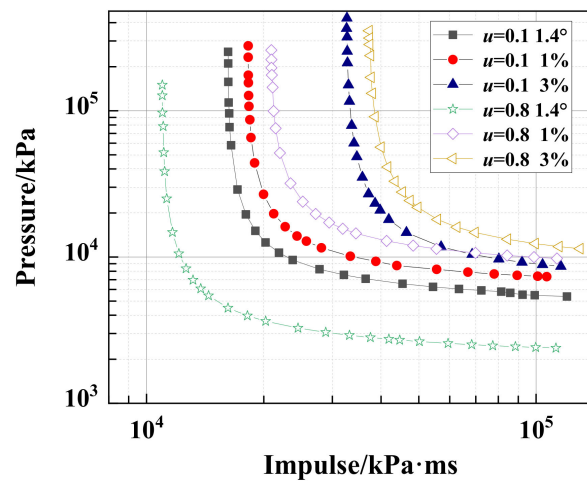


Figure 23. Analysis of P-I curves with two axial compression ratios, 0.1 and 0.8.

As shown in Figures 23 and 24, increasing the axial compression ratio could decrease the bending response asymptote, but increase the shear response asymptote. To better illustrate the variation of the asymptote, Table 13 reveals the regulation of axial compression ratio for two classifications of damage. The results show that as the axial compression ratio increases from 0.1 to 0.8, the overpressure asymptote of the bending response decreases by about 55.5% (calculated by column 2 in Table 13), and the impulse asymptote decreases by about 32.2% (calculated by column 3 in Table 13). However, for the shear response, as shown in Figure 25, as the axial compression ratio increases from 0.1 to 0.8, the overpressure asymptote increases about 33.1% and 32% (calculated by columns 4 and 6 in Table 13), and the impulse asymptote increases about 14.6% and 2.9%, (calculated by columns 5 and 7 in Table 13), respectively.

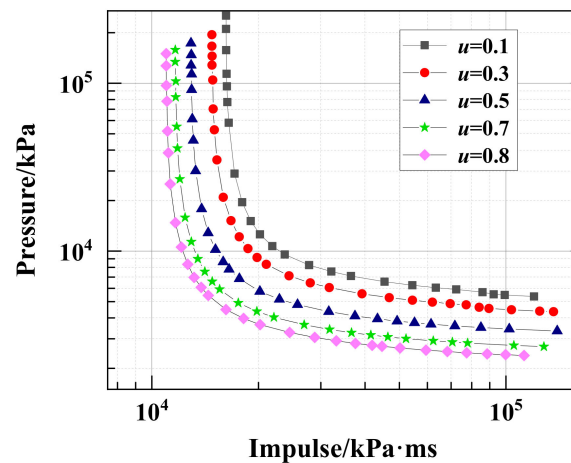


Figure 24. P-I curves of bending response with different axial compression ratios.

Table 13. Effect of axial compression ratios on asymptotes.

Axial Compression Ratios/ u	$\theta = 1.4^\circ$		$\gamma = 1\%$		$\gamma = 3\%$	
	P_0/kPa	$I_0/\text{kPa ms}$	P_0/kPa	$I_0/\text{kPa ms}$	P_0/kPa	$I_0/\text{kPa ms}$
0.1	5366	16,202	7338	18,241	8633	36,234
0.3	4355	14,477	8073	19,172	9521	34,497
0.5	3341	12,899	8816	20,075	10,319	35,878
0.7	2695	11,644	9318	20,580	10,840	36,742
0.8	2387	10,977	9770	20,912	11,396	37,277

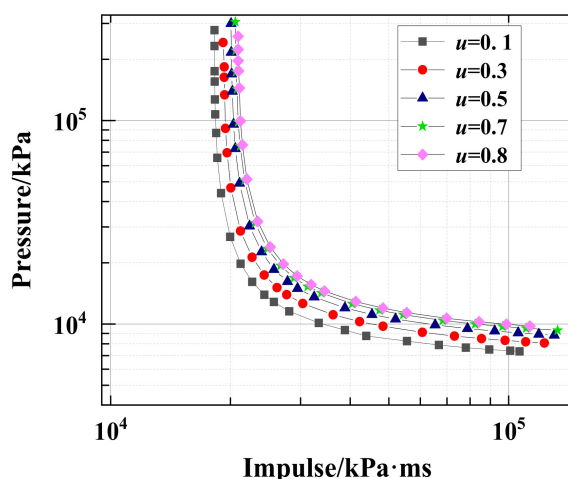


Figure 25. P-I curves for shear response with different axial compression ratios.

In summary, increasing the axial compression ratio significantly reduces the bending capacity of the RPC column. By combining with the characteristics of the load region within the P-I curve, it is inferred that reducing the axial compression ratio can effectively improve the bending capacity of the RPC column at mid-span under the blast load, i.e., reasonably reducing the axial compression ratio may effectively resist bending damage at mid-span under the blast loading.

5. Conclusions

The main conclusions of this study can be summarized as follows:

- (1) A P-I diagram approach for predicting dynamic deformation and failure modes of RPC columns subjected to blast loading is proposed.
- (2) The results show that the RPC column is susceptible to shear, bending, and bending-shear failure in the impulse load region, quasi-static load region, and dynamic load region, respectively.
- (3) The asymptotes of P-I curves increase with increasing cross-sectional dimension, RPC strength, longitudinal reinforcement ratio, and decreasing slenderness ratio and axial compression ratio.
- (4) The shape of the P-I curve of the RPC column is only related to slenderness ratio, axial compression ratio, and cross-sectional dimensions.

Author Contributions: Q.R.: Investigation; Methodology; Software; Formal analysis; Writing; Funding acquisition—original draft; Writing—review, and editing. Z.Z.: Investigation; Software; Formal analysis; Writing—review, and editing. X.H.: Methodology; Formal analysis; Writing—review, and editing; Funding acquisition. Z.J.: Writing—review, and editing. All authors have read and agreed to the published version of the manuscript.

Funding: This contribution is supported by the National Natural Science Foundation of China (No. 52078169), Excellent Youth Foundation of Heilongjiang Province (No. YQ2019E028), Outstanding Young Talents Project of Harbin University of Science and Technology (LGYC2018JQ018), and the University Nursing Program for Young Scholars with Creative Talents in Heilongjiang Province (8607-324018601).

Institutional Review Board Statement: Not applicable.

Informed Consent Statement: Not applicable.

Data Availability Statement: The data presented in this study are available on request from the corresponding author. The data are not publicly available as the data contain confidential information which cannot be publicly disclosed.

Conflicts of Interest: The authors declare no conflict of interest.

Nomenclature

K_M	Equivalent load factor
K_L	Equivalent mass factor
K_{LM}	Load-mass factor
M	Total mass of the column
C	Bending viscous damping factor of the column
$R(x)$	Bending resistance function
$F_C(t)$	External loads on the column
M_s	Shear mass of the column
R_s	Shear resistance functions
C_s	Shear viscous damping factor
$y(t)$	Shear slip deformation at support
$\ddot{y}(t)$	Shear slip acceleration at support
$\dot{y}(t)$	Shear slip speed at support
$V(t)$	Dynamic shear force at support
P	Axial compressive load
u	Axial compression ratio
N	Axial load capacity
R_m	Maximum bending resistance
Z_E	Maximum elastic displacement
Z_m	Maximum ultimate displacement
H	Height of column
\bar{R}_m	Equivalent maximum resistance
\bar{k}_e	Equivalent joint stiffness
$\frac{k_G^*}{K_L}$	Geometric stiffness
M_{ps}	Bending moment in the span
M_{pm}	Bending moment at support
$\Delta_1, \Delta_2, \Delta_3, \Delta_{max}$	Shear slip values of four stages
τ_{max}	Maximum shear strength
τ_L	Residual shear strength
K_1	Slope of model strength after cracking
K_u	Slope of shear strength after exceeding the maximum value
θ_{max}	Maximum rotating angle at column end
Δ_{max}	Maximum lateral deflection in the span
γ	Average shear strain in the shear deformation zone
γ_s	Accumulated shear slip magnitude in the shear deformation zone
e	Half-width of the shear deformation zone
L	Length of column cross-section
B	Height of column cross-section
f_c	Standard values for axial compressive strength
ρ	Longitudinal reinforcement rate
P_0	Overpressure asymptote threshold
I_0	Impulse asymptote threshold

References

1. UFC 3-340-02; Structures to Resist the Effects of Accidental Explosions. U.S. Department Defense: Washington, DC, USA, 2008. Available online: https://www.wbdg.org/FFC/DOD/UFC/ARCHIVES/ufc_3_340_02.pdf (accessed on 5 December 2008).
2. Cao, S.; Hou, X.; Rong, Q. Dynamic compressive properties of reactive powder concrete at high temperature: A review. *Cem. Concr. Compos.* **2020**, *110*, 103568. [\[CrossRef\]](#)
3. Yi, N.; Kim, J.H.J.; Han, T.; Cho, Y.-G.; Lee, J.H. Blast-resistant characteristics of ultra-high strength concrete and reactive powder concrete. *Constr. Build. Mater.* **2012**, *28*, 694–707. [\[CrossRef\]](#)
4. Hou, X.; Cao, S.; Rong, Q.; Zheng, W.; Li, G. Effects of steel fiber and strain rate on the dynamic compressive stress-strain relationship in reactive powder concrete. *Constr. Build. Mater.* **2018**, *170*, 570–581. [\[CrossRef\]](#)
5. Wang, Y.; Wang, Z.; Liang, X.; An, M. Experimental and numerical studies on dynamic compressive behavior of reactive powder concretes. *Acta Mech. Solida Sin.* **2008**, *21*, 420–430. [\[CrossRef\]](#)
6. Wu, Z.; Shi, C.; He, W.; Wang, D. Static and dynamic compressive properties of ultra-high performance concrete (UHPC) with hybrid steel fiber reinforcements. *Cem. Concr. Compos.* **2017**, *79*, 148–157. [\[CrossRef\]](#)

7. Ren, X.; Zhou, T.; Zhong, F.; Hu, Y.; Wang, W. Dynamic mechanical behavior of steel-fiber reactive powder concrete. *Explos. Shock*. **2011**, *31*, 540–547.
8. Jiao, C.; Sun, W. Impact resistance of reactive powder concrete. *J. Wuhan Univ. Technol.-Mater. Sci. Ed.* **2015**, *30*, 752–757. [[CrossRef](#)]
9. Ju, Y.; Liu, H.; Sheng, G.; Wang, H. Experimental study of dynamic mechanical properties of reactive powder concrete under high-strain-rate impacts. *Sci. China Technol. Sci.* **2010**, *53*, 2435–2449. [[CrossRef](#)]
10. Fujikake, K.; Senga, T.; Ueda, N.; Ohno, T.; Katagiri, M. Study on impact response of reactive powder concrete beam and its analytical model. *Adv. Concr. Technol.* **2006**, *4*, 99–108. [[CrossRef](#)]
11. Fujikake, K.; Senga, T.; Ueda, N.; Ohno, T.; Katagiri, M. Nonlinear analysis for reactive powder concrete beams under rapid flexural loadings. *Adv. Concr. Technol.* **2006**, *4*, 85–97. [[CrossRef](#)]
12. Kou, J.; Gong, Z. Experimental study on the impact resistance of reactive powder concrete slabs. *Earthq. Eng. Eng. Vib.* **2020**, *40*, 133–144. (In Chinese)
13. Hou, X.; Cao, S.; Rong, Q.; Zheng, W. A P-I diagram approach for predicting failure modes of RPC one-way slabs subjected to blast loading. *Int. J. Impact Eng.* **2018**, *120*, 171–184. [[CrossRef](#)]
14. Li, J.; Wu, C.; Hao, H. Residual loading capacity of ultra-high performance concrete columns after blast loads. *Int. J. Prot. Struct.* **2015**, *6*, 649–670. [[CrossRef](#)]
15. Li, J.; Wu, C.; Hao, H.; Liu, Z. Post-blast capacity of ultra-high performance concrete columns. *Eng. Struct.* **2017**, *134*, 289–302. [[CrossRef](#)]
16. Mai, V.-C.; Luu, X.-B.; Dao, C.-B.; Le, D.V. Investigate the structural response of ultra-high performance concrete column under the high explosion. *Def. Sci. J.* **2021**, *71*, 256–264. [[CrossRef](#)]
17. Krauthammer, T.; Astarlioglu, S.; Blaskoa, J.; Soh, T.B.; Ng, P.H. *Load-Impulse Diagrams of Reinforced Concrete Beams Subjected to Concentrated Transient Loading*; Technical Report: PTC-TR-006-2004; Pennsylvania State University: State College, PA, USA, 2004.
18. Fischer, K.; Häring, I. SDOF response model parameters from dynamic blast loading experiments. *Eng. Struct.* **2009**, *31*, 1677–1686. [[CrossRef](#)]
19. Yang, G.; Lok, T.-S. Analysis of RC structures subjected to air-blast loading accounting for strain rate effect of steel reinforcement. *Int. J. Impact Eng.* **2006**, *34*, 1924–1935. [[CrossRef](#)]
20. Sun, J.; Li, G.; Lu, Y. Equivalent single degree of freedom model of SRC columns under blast loading. *J. Vib. Shock*. **2007**, *26*, 82–89.
21. Biggs, J.M. *Introduction to Structural Dynamics*; McGraw-Hill: New York, NY, USA, 1964.
22. Wu, P. *Study on the Effect of Axial Compression Ratio on the Blast Resistance of Steel Pipe Concrete Columns*; Chang'an University: Xian, China, 2014. (In Chinese)
23. Clough, R.W.; Penzien, J. *Structural Dynamics*, 2nd ed.; Higher Education Publishers: Beijing, China, 2006.
24. Li, Q.; Meng, H. Pressure-impulse diagram for blast loads based on dimensional analysis and single-degree-of-freedom model. *J. Eng. Mech.* **2002**, *128*, 87–92. [[CrossRef](#)]
25. Li, Q.; Meng, H. Pulse loading shape effects on pressure-impulse diagram of an elastic-plastic, single-degree-of-freedom structural model. *Int. J. Mech. Sci.* **2002**, *44*, 1985–1998. [[CrossRef](#)]
26. Fallah, A.S.; Louca, L.A. Pressure-impulse diagrams for elastic-plastic-hardening and softening single-degree-of-freedom models subjected to blast loading. *Int. J. Impact Eng.* **2007**, *34*, 823–842. [[CrossRef](#)]
27. Colombo, M.; Martinelli, P. Pressure-impulse diagrams for RC and FRC circular plates under blast loads. *Eur. J. Environ. Civ. Eng.* **2012**, *16*, 837–862. [[CrossRef](#)]
28. Krauthammer, T.; Bazeos, N.; Holmquist, T.J. Modified SDOF analysis of RC box-type structures. *J. Struct. Eng.* **1986**, *112*, 726–744. [[CrossRef](#)]
29. Malvar, L.J. Review of static and dynamic properties of steel reinforcing bars. *ACI Mater. J.* **1998**, *95*, 609–616.
30. Xu, J.; Wu, C.; Xiang, H.; Su, Y.; Li, Z.-H.; Fang, Q.; Hao, H.; Liu, Z.; Zhang, Y.; Li, J. Behaviour of ultra-high performance fiber reinforced concrete columns subjected to blast loading. *Eng. Struct.* **2016**, *118*, 97–107. [[CrossRef](#)]
31. Astarlioglu, S.; Krauthammer, T. Response of normal-strength and ultra-high-performance fiber-reinforced concrete columns to idealized blast loads. *Eng. Struct.* **2014**, *61*, 1–12. [[CrossRef](#)]
32. Ma, G.; Shi, H.; Shu, D. P-I diagram method for combined failure modes of rigid-plastic beams. *Int. J. Impact Eng.* **2007**, *34*, 1081–1094. [[CrossRef](#)]
33. Wang, W.; Zhang, D.; Lu, F.; Tang, F.-J.; Wang, S.-C. Pressure-impulse diagram with multiple failure modes of one-way reinforced concrete slab under blast loading using SDOF method. *J. Cent. South Univ.* **2013**, *20*, 510–519. [[CrossRef](#)]
34. Huang, X.; Bao, H.; Hao, Y.; Hao, H. Damage assessment of two-way RC slab subjected to blast load using mode approximation approach. *Int. J. Struct. Stab. Dyn.* **2017**, *17*, 1750013. [[CrossRef](#)]
35. Shi, Y.; Hao, H.; Li, Z. Numerical derivation of pressure-impulse diagrams for prediction of RC column damage to blast loads. *Int. J. Impact Eng.* **2008**, *35*, 1213–1227. [[CrossRef](#)]
36. Zhang, F.; Wu, C.; Zhao, X.; Li, Z.-X. Numerical derivation of pressure-impulse diagrams for square UHPCFDST columns. *Thin-Walled Struct.* **2017**, *115*, 188–195. [[CrossRef](#)]
37. Wang, W. *Study of the Damage Effect and Assessment Method of Reinforced Concrete Structural Member under Blast Loading*; National University of Defense Technology: Beijing, China, 2012. (In Chinese)
38. *GB/T50010-2010*; Code for Design of Concrete Structures. Ministry of Housing and Urban-Rural Development of the People's Republic of China. China Architecture & Building Press: Beijing, China, 2010. (In Chinese)

39. Lv, X.; Wang, Y.; Fu, C.; Zheng, W. Basic mechanical property indexes of reactive powder concrete. *J. Harbin Inst. Technol.* **2014**, *46*, 1–9.
40. Rong, Q.; Zeng, Y.; Hou, X.; Zheng, W. Experimental study on mechanical behavior of RPC-filled circular steel tube columns under axial compression. *J. Build. Struct.* **2019**, *40*, 247–253.
41. *GB/T50011-2018*; Code for Seismic Structural Design of Building Structures. Ministry of Housing and Urban-Rural Development of the People's Republic of China. China Architecture & Building Press: Beijing, China, 2018. (In Chinese)